Journal of Applied Physics

Mechanical properties of hydrogenated amorphous silicon (a-Si:H) particles

Cite as: J. Appl. Phys. **126**, 204303 (2019); https://doi.org/10.1063/1.5117282
Submitted: 02 July 2019 . Accepted: 09 November 2019 . Published Online: 26 November 2019

Taizhi Jiang, Fardin Khabaz, Aniket Marne, Chenglin Wu, Raluca Gearba, Revanth Bodepudi, Roger T. Bonnecaze, Kenneth M. Liechti, and Brian A. Korgel

Journal of Applied Physics ARTICLE scitation.org/journal/jap

Mechanical properties of hydrogenated amorphous silicon (a-Si:H) particles

Cite as: J. Appl. Phys. **126**, 204303 (2019); doi: 10.1063/1.5117282
Submitted: 2 July 2019 · Accepted: 9 November 2019 ·
Published Online: 26 November 2019

Taizhi Jiang,[1,2] Fardin Khabaz,[1] Aniket Marne,[2] Chenglin Wu,[3] Raluca Gearba,[2] Revanth Bodepudi,[4] Roger T. Bonnecaze,[1] Kenneth M. Liechti,[2,4] and Brian A. Korgel[1,2,a)]

AFFILIATIONS

[1]McKetta Department of Chemical Engineering, The University of Texas at Austin, Austin, Texas 78712-1062, USA
[2]Materials Science and Engineering Program and Texas Materials Institute, The University of Texas at Austin, Austin, Texas 78712-1591, USA
[3]Department of Civil, Architectural, and Environmental Engineering, Missouri University of Science and Technology, Rolla, Missouri 65409, USA
[4]Department of Aerospace Engineering and Engineering Mechanics, The University of Texas at Austin, Austin, Texas 78712, USA

[a)]**Author to whom correspondence should be addressed:** korgel@che.utexas.edu

ABSTRACT

A nanoindenter was used to compress individual particles of hydrogenated amorphous silicon (a-Si:H) ranging in diameter from 290 nm to 780 nm. The colloidal synthesis used to produce the particles enables the hydrogen content to be manipulated over a wide range, from about 5 at. % to 50 at. %, making these a-Si:H particles promising for applications in lithium ion batteries, hydrogen storage, and optical metamaterials. Force-displacement curves generated using a tungsten probe flattened with focused ion beam exhibited elastic and then plastic deformations, followed by fracture and crushing of the particles. For particles with 5% and 50% H, Young's moduli, yield strengths, and compressive strengths were 73.5(±19.5) GPa, 5.8 GPa, and 3.2(±0.1)–9.3(±0.6) GPa and 31.2(±9.0) GPa, 2.5 GPa, and 1.8 (±0.3)–5.3 (±0.8) GPa, respectively. Particles with more hydrogen were significantly more compliant and weaker. This is consistent with atomistically detailed molecular dynamics simulations, which revealed compression forms of an interphase of H atom clusters that weakens the material.

I. INTRODUCTION

Colloidal particles of hydrogenated amorphous silicon (a-Si:H) can be synthesized with a spherical shape and a uniform diameter from about 280 nm to more than 1 μm, with hydrogen content that can be varied widely from a few percent to nearly 60 at. %.[1,2] The optical gap of a-Si:H depends on the hydrogen content and the extent of amorphization, making it possible to tune the color of the colloids from bright yellow to orange to red to dark brown/black.[2] The high refractive index of Si and the absence of long wavelength light absorption typical of metals make them especially interesting for photonic applications and metamaterial assembly.[3–6] The particles might also be useful for H storage or fuel cells[2] and have been studied as negative electrode materials in lithium ion batteries (LIBs).[7,8] For LIBs, the particles have been observed to undergo significant expansion and compression during each lithiation and delithiation cycle without pulverization;[8] however, the mechanical properties of these particles have not yet been measured.

Here, we report the first mechanical property measurements of individual colloidal a-Si:H particles with submicrometer size. For these measurements, we initially considered using an atomic force microscope (AFM), as it provides a convenient way to find individual particles on a substrate and has actually been used to study the mechanical properties of other materials with nanoscale resolution, including various kinds of nanowires/nanofibers,[9–11] thin films,[12–15] and organic/biomaterials.[16–19] Those materials, however, are all relatively soft compared to a-Si:H particles, and the load capacity of an AFM was not sufficient to make the measurements. For instance, a-Si and crystalline Si (c-Si) are relatively stiff and strong materials, as bulk a-Si and thin films have Young's moduli ranging from 60 to 140 GPa,[20–23] and bulk crystalline Si (c-Si) and a-Si:H thin films have ultimate compressive strengths of

15–25 GPa[24,25] and ~1 GPa,[22,26,27] respectively. We found that mechanical compression tests could be carried out on individual a-Si:H particles using a nanoindenter equipped with a stiff tungsten (W) probe with a flattened tip of 10 μm diameter. The force-displacement (*F-D*) curves showed regimes of elastic deformation, plastic deformation (yielding), and fracture (or crushing). Young's modulus, yield strength, and ultimate compressive strength were found to decrease when more hydrogen was incorporated in the particles. The mechanical response of the particles was modeled using atomistically detailed molecular dynamics (MD) simulations. These simulations revealed that mechanical compression leads to the formation of an interphase of clustered H, which appears to be responsible for the observed softening and weakening of the material with increased H content.

II. EXPERIMENTAL DETAILS

A. Materials

Trisilane (Si_3H_8, 100%) was purchased from Voltaix. (Caution: Trisilane is a pyrophoric liquid and should be stored and handled with caution under an inert atmosphere. When used in a glove box, the oxygen level should be <1 ppm). Chloroform ($CHCl_3$, 99.9%) and *n*-hexane (C_6H_{14}, anhydrous, 95%) were purchased from Sigma-Aldrich and *p*-type boron-doped Si wafers (100) (resist: 9–10 Ω cm) were purchased from University Wafer. All chemicals were used as received.

B. a-Si:H particle synthesis and characterization

Colloidal particles of a-Si:H were synthesized by thermal decomposition of trisilane in supercritical *n*-hexane at 34.5 MPa (5000 psi).[1,2] The reaction temperature determines that the H content was varied from 380 °C to 470 °C to make the samples.[2] All reactions were carried out in a sealed high pressure titanium reactor with a volume of 10 ml. Trisilane (21 μl) and *n*-hexane are added to the reactor in a nitrogen-filled glove box. The amount of *n*-hexane added for each reaction is determined by the reaction temperature based on its phase diagram in order to maintain a reaction pressure of 34.5 MPa.[28] For example, reactions at 380 °C and 470 °C require 6.4 ml and 5.5 ml of hexane, respectively. After sealing the reactor, it is removed from the glove box and placed into a heating block and then heated at about 70–90 °C/min to reach the target temperature. The reaction is held at the desired temperature for 5 min and then immersed in an ice bath until it has cooled enough for handling—usually about 20 min. The crude reaction product is then centrifuged at 8000 rpm (8228 rcf) for 5 min to isolate the particles from soluble reaction byproducts. The supernatant is discarded and the precipitate is redispersed in 20 ml of chloroform. The particles are washed two more times by centrifugation at 8000 rpm (8228 rcf) for 5 min and redispersion of the precipitate in 20 ml of chloroform. The final product of colloidal a-Si:H particles is dispersed in chloroform and stored at room temperature in air.

Powder X-ray diffraction (XRD) data were acquired using a Rigaku R-Axis Spider diffractometer operated at 40 kV and 40 mA with X-ray from a Cu Kα source (λ = 1.54 Å). A few drops of colloidal dispersion are dried on a glass substrate and then particles are collected onto a 0.5 mm nylon loop dipped into mineral oil to facilitate particle collection. The sample was rotated at 5 deg s^{-1}. Background subtraction and data processing were carried out using Rigaku 2DP software.C.

C. Nanoindentation

Mechanical compression tests were performed using an MTS NANO Indenter XP, KLA-Tencor. The nanoindenter probe was prepared in two steps. A 250 μm diameter W wire was electrochemically etched in a 1 M KOH solution to generate a tip with a radius of curvature of ~200 nm.[29] The tip was then cut in an FEI Strata™ DB235 dual beam system with gallium ions (1 nA, 30 kV) to obtain a flat end with 10 μm diameter and then polished using beams with gradually reduced currents of 500 pA, 300 pA, and 100 pA.

Samples were prepared by casting a-Si:H particles onto a 1×1 cm^2 Si (100) wafer from a colloidal dispersion in chloroform with a concentration of ~50 μg/ml. Before depositing the particles, the Si wafer was sonicated in chloroform for 5 min and dried with compressed air. Individual particles were found for testing using SEM imaging (Zeiss Supra 40 SEM). To avoid indenting more than one particle at a time, the target particle had to be at least 10 μm away from any other particles. Measurements were taken using a tip approaching speed of 30 nm/s and a stiffness sensitivity of 125 N/m.

D. Molecular dynamics simulations

Atomistically detailed molecular dynamics (MD) simulations of the structure and mechanical properties of a-Si:H with 5%, 10%, 20%, 30%, and 50% hydrogenation (atomic fraction) were carried out. Thirty-thousand Si atoms were placed on a diamond-cubic lattice with a density of 2.32 g/cm^3 in a periodic box. Interatomic interactions between Si-Si, Si-H, and H-H atoms were determined using the Tersoff potential,[30,31] which takes account of three-body interactions in the calculation of the potential energy of the system. Following methods used in MD simulations of various glass-forming materials,[32,33] c-Si was heated to $T > 1800$ K in an isothermal-isobaric ensemble (constant number of atoms, pressure, and temperature, i.e., NPT ensemble) to liquid Si. The system was quenched with a rate of 50 K/ns to an amorphous structure at $T = 300$ K and P = 1 bar. The pair distribution function was used to ensure that the final structure is a glass (see Fig. S8b in the supplementary material). Hydrogen atoms were added to Si sites with a dangling bond, i.e., coordination number less than four, to generate a-Si:H. Starting with atoms with a single dangling bond, H atoms were added to preserve the tetrahedral bonding of the Si atoms at a distance of 1–1.2 Å as suggested by Biswas *et al.*[34] All of the equilibrium MD runs were performed with 1 bar pressure and time steps of 0.1–1 fs using the LAMMPS package.[35] Systems with 60 000 and 120 000 atoms also lead to similar results.

Structures of a-Si and a-Si:H equilibrated at $T = 300$ K and $P = 1$ bar were used to characterize the effect of hydrogenation on the mechanical properties of these systems. Before applying tensile deformation to the MD sample, we ensured that residual stress was removed by applying a short NPT ensemble simulation with a constant number of atoms, pressure, and temperature for the periodic box lengths to relax independently at 1 bar of pressure.

This simulation was then followed by a uniaxial deformation. The faces perpendicular to the applied strain were subjected to 1 bar; the lengths of these faces perpendicular to the applied strain are allowed to change under the tensile deformation. Maximum strain (ε_{max}) values of 0.05 and 0.5 were used to perform the tensile deformation in a-Si and a-Si:H systems, respectively. This simulation was followed by a uniaxial deformation, in which one dimension of the box was deformed with a rate of $10^8\ s^{-1}$. Compressive deformation produced similar values of Young's modulus.

III. RESULTS AND DISCUSSION

A. Synthesis of a-Si:H particles

Colloidal particles of a-Si:H were synthesized by the thermal decomposition of Si_3H_8 in supercritical *n*-hexane as shown in Fig. 1(a). Three different samples were made for this study, with [H]/[H + Si] contents of 5%, 10%, and 50%. Figure 1(b) shows photographs of the a-Si:H samples dispersed in chloroform. Their color depends on the H content of the particles.[2,36,37] Particles with very high H content appear yellow, whereas the particles with the least amount of H appear nearly black and particles in the middle have a red hue to them. The H content also affects the refractive index of the particles and shifts the scattering spectral features toward visible wavelengths.[6] The reaction temperature used to degrade trisilane determines the extent of hydrogen loss from the reactant and the hydrogen content of the product. Nearly complete removal of H occurs at the highest reaction temperature of 450°C, but there is still not enough thermal energy to crystallize the Si. Figure S1 in the supplementary material shows XRD data for the particles, confirming their amorphous structure. At the lowest reaction temperature of 380°C, very little H is lost during particle nucleation and growth.

The a-Si:H particles formed by this colloidal approach are spherical and uniform in size. Figures 1(c)–1(e) show SEM images of the a-Si:H particles used in this study. The H content of the a-Si:H particles reported here is an estimate based on their color using

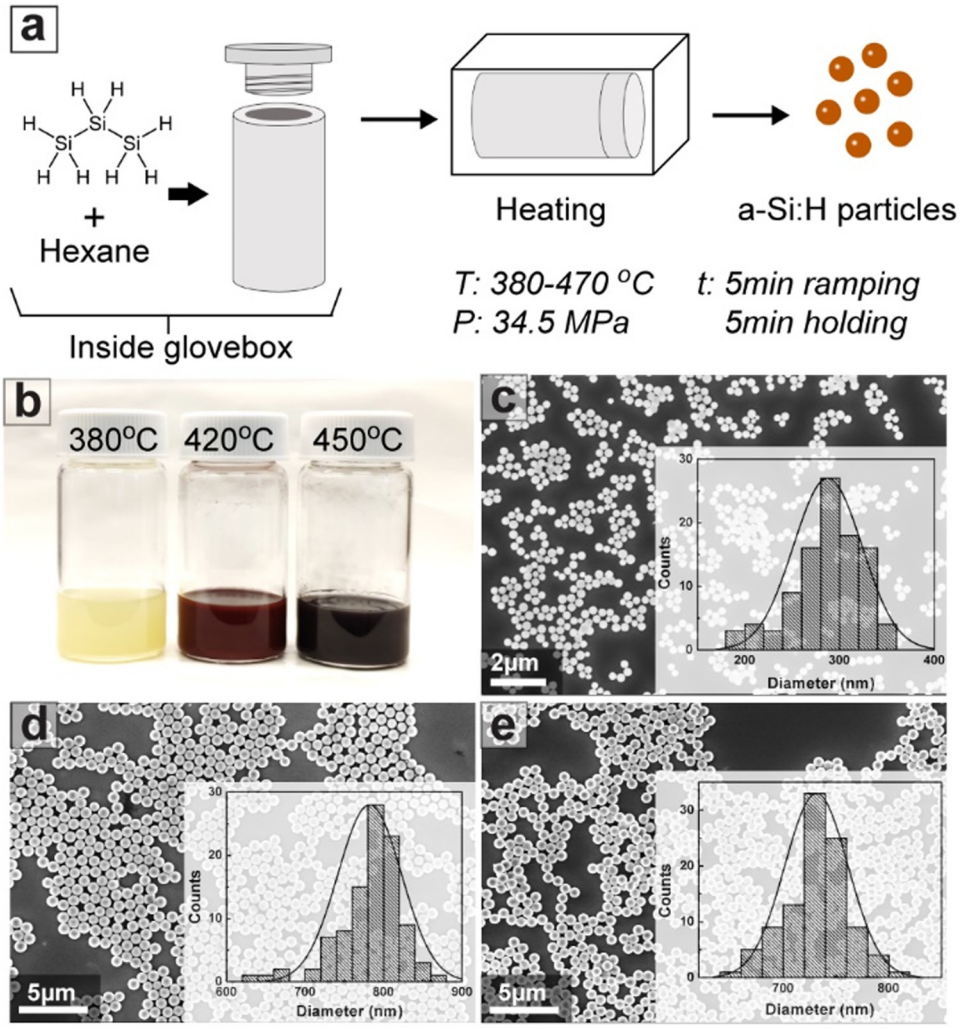

FIG. 1. (a) Illustration of the a-Si:H particle synthesis. The reaction is carried out at 34.5 MPa at a range of temperatures. The reaction temperature determines the extent of hydrogenation of the particles. (b) A photograph of colloidal a-Si:H dispersions in chloroform made at the indicated temperatures. The difference in color results from the amount of H incorporated into the particles. The particles made at 380 °C, 420 °C, and 450 °C have compositions of $Si_{0.5}H_{0.5}$, $Si_{0.9}H_{0.1}$, and $Si_{0.95}H_{0.05}$, respectively. (c)–(e) SEM images of the a-Si:H particles made at (c) 380 °C, (d) 420 °C, and (e) 450 °C. The size histograms of each sample are included as insets, with average diameters and standard deviations about the mean of 287.5 ± 36.1 nm, 782.3 ± 40.6 nm, and 731.5 ± 30 nm.

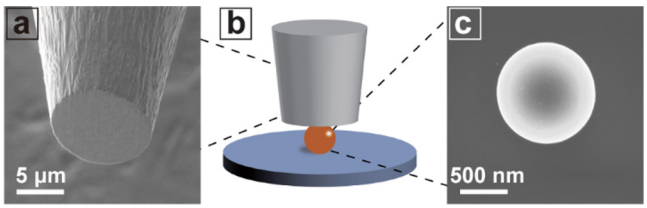

FIG. 2. (a) SEM image of a W nanoindenter tip used to carry out single particle compression tests. (b) Illustration of the single particle experiment. The tip has a diameter of 10 μm, and the particle diameters ranged from 290 nm to 780 nm. (c) SEM image of a 1.04 μm diameter a-Si:H particle ($Si_{0.95}H_{0.05}$) that was tested.

the correlation between color and the H content reported in our previous work.[2] Particles synthesized at 380 °C, 420 °C, and 450 °C have compositions of 50 at. % H ($Si_{0.5}H_{0.5}$), 10 at. % H ($Si_{0.9}H_{0.1}$), and 5 at. % H ($Si_{0.95}H_{0.05}$), respectively. The average diameters of these particles were determined by SEM: 287.5 ± 36.1 nm, 782.3 ± 40.6 nm, and 731.5 ± 30 nm. The particles with the highest H content have a significantly smaller diameter than the particles with a low H content because it is not possible to independently control both size and H content during the reaction.

B. Nanoindentation of individual a-Si:H particles

An SEM image of a W probe with a flat, polished tip used to compress the particles is shown in Fig. 2(a). Figure 2(b) illustrates the compression experiment, and Fig. 2(c) shows an SEM image of one of the a-Si:H particles that were compressed on a Si (100) substrate. This particle is 1.04 μm in diameter with a composition of $Si_{0.95}H_{0.05}$.

Figure 3 shows SEM and optical microscopy images of an individual a-Si:H particle before and after nanoindentation. A combination of SEM and optical microscopy was used to identify and locate particles for testing. SEM was then used again to confirm that only the one particle of interest was compressed during the experiment. Figure 3(a) shows an SEM image of a region of a-Si:H particles that was identified as a reference spot, large enough to find under the optical microscope attached to the nanoindenter, that served as a spatial reference to map the location of the individual, isolated particle to be tested. For these experiments, the collection of a-Si:H particles needed to cover a substrate area of about 200 × 200 μm^2 to be easily identified under the microscope. Once the cluster or region of aggregated particles was found, an isolated particle separated from the group was identified as highlighted with the box in Fig. 3(b). Once the particle of interest was found, several SEM images were taken to map precisely its position so it could be located under the optical microscope on the nanoindenter.

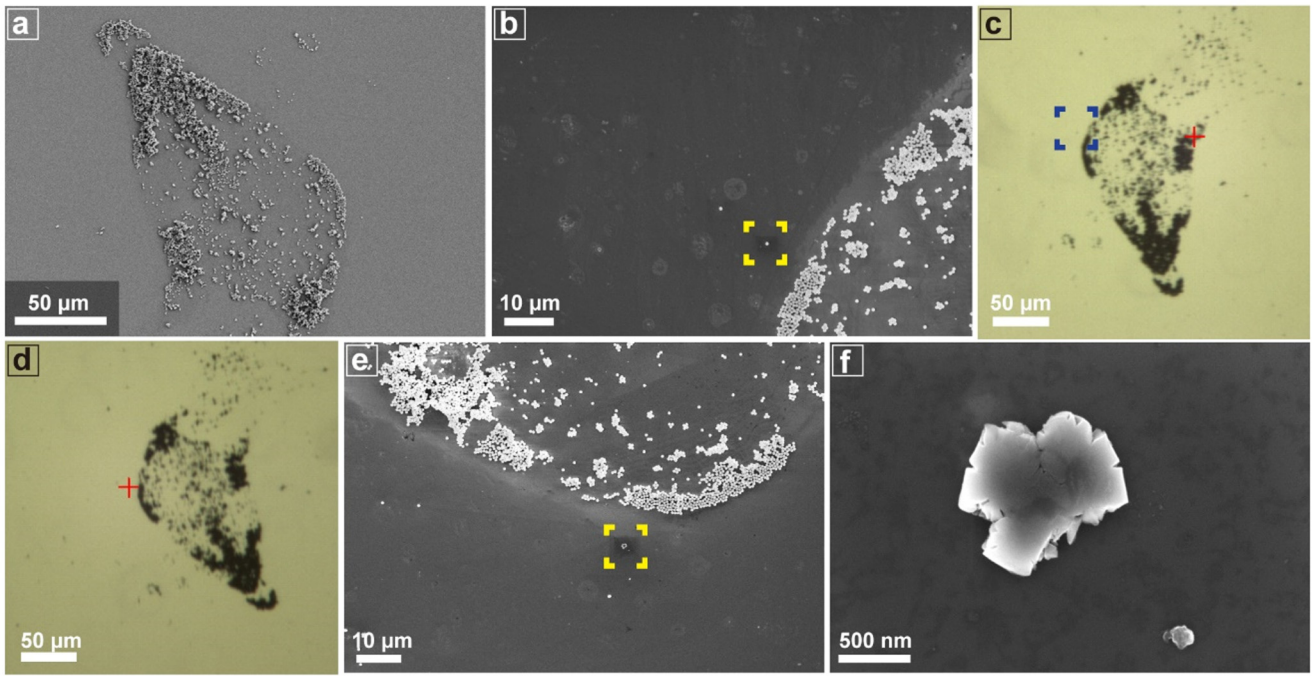

FIG. 3. Locating a single particle and performing nanoindentation. (a) SEM image of a cluster of a-Si:H particles covering a substrate area of 200 × 200 μm^2. (b) An SEM image showing an isolated particle (in the yellow box) that was identified for mechanical testing. (c)–(d) Images from the optical microscope on the nanoindenter corresponding to the cluster of particles in the SEM image in (a). In (d), the particle identified for mechanical testing is indicated with the red cross. The red cross indicates the exact spot for nanoindentation. This is the particle indicated by the yellow box in (b). (e) and (f) SEM images of the fractured particle after indentation.

Figures 3(c) and 3(d) show the images of this cluster of particles obtained under the optical microscope on the nanoindenter. The map created by SEM was then used to determine the position of the individual particle and to position the nanoindenter. Often, multiple individual particles were labeled if they satisfied the distance requirement, so several particles could be studied during each run. By referring to the SEM images with individual particle labels, each individual particle could be found, and the particle position was recorded as the nanoindentation coordinates, which is the red cross in Fig. 3(d). After performing the experiments, the Si wafer was imaged by SEM to confirm that only an individual particle was indented and completely fractured. Figures 3(e) and 3(f) show SEM images of the particle found in Fig. 3(b) after crushing it in the compression test. The shape of the force profiles also provided confirmation that only a single particle had been tested. When multiple particles were positioned under the tip, the force profile exhibited discontinuities, signaling that multiple particles were compressed by the tip (see Fig. S2 in the supplementary material).

C. Elastic deformation

Figure 4(a) shows an example of a force profile obtained from a single particle of $Si_{0.95}H_{0.05}$ with a diameter of 730 nm. It also shows the strain (ε, defined as the displacement divided by the particle diameter) corresponding to displacement (D) along the top of the graph. When the particle is compressed, it undergoes elastic deformation until reaching a yield point when plastic deformation ensues, defined by a noticeable drop in the slope of the force profile. The extent of plastic deformation then increased until fracture. A final displacement equal to ½ the particle diameter was set for all of the measurements. After reaching this value, the tip was retracted and the fractured particle experienced unloading. The deformation recovered elastically until the tip had no interaction with the particle. Figure 4(a) shows a typical force profile for a semibrittle material, where nonlinear behavior is seen just before fracture while there is no stress-whitening after fracture.[38] The a-Si:H particles exhibit a significant amount of ductility and plastic deformation. The maximum strain (fracture strain) in Fig. 4(a) is much larger than the value for a bulk c-Si (<2.5%).[39,40] Table I provides all of the average maximum strains for the particles that were tested.

Young's moduli were calculated from the force profiles using Hertzian theory.[41,42] For Hertzian theory to apply, the contact area must be small compared to the tip radius, the Si wafer substrate, and the a-Si:H particle radius, and there can be no friction between the particle and the two planes in the contact area. Hertzian theory can usually be applied when the strain is less than 1%–10%.[41,43] The contact radius at interface 1, a_1, is

$$a_1 = \sqrt{R\delta_1} = \left(\frac{3}{4}\frac{R}{E^*}F\right)^{1/3}. \quad (1)$$

The interface between the Si wafer and the a-Si:H particle is noted by the subscript "1." The subscript "2" is used for the interface between a-Si:H particle and W tip. R is the radius of a-Si:H particle, δ_1 is the deformation on the interface of the Si substrate and the a-Si:H particle, F is the compressive force, and E^* is

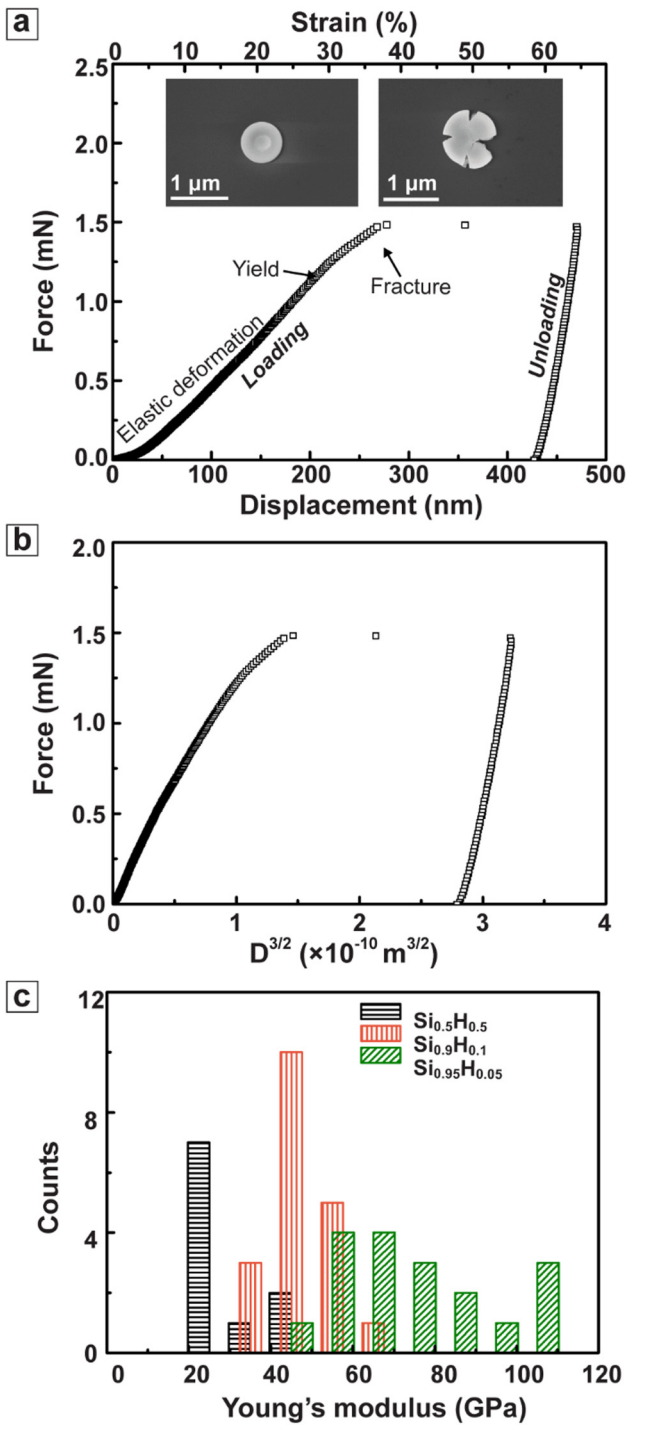

FIG. 4. (a) Single particle force profile of a $Si_{0.95}H_{0.05}$ particle (with a diameter of 730 nm). The strain, ε, is defined as the displacement divided by the particle diameter. (Inset) SEM images of the corresponding a-Si:H particle before and after nanoindentation. (b) F-$D^{3/2}$ curves of the a-Si:H particle shown in Fig. 4(a). (c) Distribution of Young's moduli obtained from all the tests.

TABLE I. The diameter, maximum strain, and mechanical properties of a-Si:H particles with three different H contents, a-Si thin films, and bulk c-Si.

	Diameter (nm)	Maximum strain (%)	Young's modulus (GPa)	Yield strength (GPa)	Compressive strength (min) (GPa)	Compressive strength (max) (GPa)
$Si_{0.5}H_{0.5}$	287.5 ± 36.1	36.7 ± 4.8	31.2 ± 9.0	2.5	1.8 ± 0.3	5.3 ± 0.8
$Si_{0.9}H_{0.1}$	782.3 ± 40.6	39.1 ± 1.8	46.5 ± 7.6	4.6	2.7 ± 0.1	7.6 ± 0.4
$Si_{0.95}H_{0.05}$	731.5 ± 30.0	34.0 ± 1.4	73.5 ± 19.5	5.8	3.2 ± 0.1	9.3 ± 0.6
a-Si thin films	…	…	60–140[21–23]	~1[47]	~1[22,26,27]	
Bulk c-Si	…	<2.5[39,40]–	120–190[48,49]	7[50]	15–25[24,25]	

the reduced Young's modulus. Rearranging Eq. (1) generates Eqs. (2) and (3),

$$\delta_1 = \left(\frac{3}{4}\frac{F}{E^*\sqrt{R}}\right)^{2/3}, \tag{2}$$

$$E^* = \frac{3}{4}\delta_1^{-\frac{3}{2}}\frac{F}{\sqrt{R}}. \tag{3}$$

E^* is related to Young's moduli of the a-Si:H particle and the Si substrate, E_p and E_{sub}, and their Poisson's ratios, ν_p and ν_{sub},

$$\frac{1}{E^*} = \frac{1-\nu_p^2}{E_p} + \frac{1-\nu_{sub}^2}{E_{sub}}. \tag{4}$$

Poisson's ratio of 0.22 for amorphous Si was used.[23,44] Note that, in this range, the value of Poisson's ratio has little impact on the value of Young's modulus calculated by Eq. (4).[41] Values of 130 GPa for E_{sub} and 0.22 for ν_{sub} were used.[41] Combining Eqs. (3) and (4) gives Eq. (5). Equation (6) applies to the interface between the a-Si:H particle and W tip (interface 2), and value for Young's modulus of W, E_w, was 400 GPa, and Poisson's ratio of W, ν_w, was 0.27. δ_2 is the deformation on the W tip surface and the a-Si:H particle interface,

$$\frac{1}{E^*} = \frac{1-\nu_p^2}{E_p} + \frac{1-\nu_{sub}^2}{E_{sub}} = \frac{4}{3}\delta_1^{3/2}\frac{\sqrt{R}}{F}, \tag{5}$$

$$\frac{1}{E^*} = \frac{1-\nu_p^2}{E_p} + \frac{1-\nu_w^2}{E_w} = \frac{4}{3}\delta_2^{3/2}\frac{\sqrt{R}}{F}. \tag{6}$$

The displacement, D, is the sum of the deformation at both interfaces, δ_1 and δ_2. By combining and rearranging Eqs. (5) and (6),

$$F = \frac{4}{3}\sqrt{R}\left(\frac{1-\nu_{sub}^2}{E_{sub}} + \frac{1-\nu_w^2}{E_w}\right)^{-1}\left[\left(\frac{\delta_1}{D}\right)^{3/2} - \left(\frac{\delta_2}{D}\right)^{3/2}\right]D^{3/2}, \tag{7}$$

$$\delta_1 + \delta_2 = D. \tag{8}$$

Equation (7) shows that F is proportional to $D^{3/2}$, provided that the deformation of each interface, δ_1 and δ_2, is proportional to the total deformation, D. Figure 4(b) shows the force profiles in Fig. 4(a) replotted as F vs $D^{3/2}$. The resulting curve is initially linear, as expected based on Eq. (7), and suggests that the behavior is elastic at the beginning of the compression experiment. Further evidence of this initially elastic response is provided by experiments that were conducted with loading and unloading the Si particles to a smaller depth, as shown in Fig. S3 in the supplementary material. In the linear range of F-$D^{3/2}$ curves, the particles are undergoing elastic deformation. Young's modulus of the particles was calculated from the slope of the curves in the linear regime where Hertzian theory is valid. Table I summarizes the values obtained by averaging the measurements of at least 10 particles per sample. The force profiles for all these particles are given in the supplementary material. Figure 4(c) shows Young's moduli distribution that was obtained from all the tests.

D. Plastic deformation

Deviation from linearity in the F vs $D^{3/2}$ curves indicates that the material begins to undergo plastic (nonreversible) deformation. Figure 5 shows the force profiles from three representative measurements of the $Si_{0.5}H_{0.5}$, $Si_{0.9}H_{0.1}$, and $Si_{0.95}H_{0.05}$ particles. The yield point was estimated by comparing the experimental data with the Hertzian model [Eq. (7)] for the elastic response. The threshold for divergence was set to a 10% difference in the slopes of the two responses. After identifying force and displacement values for the onset of yield, the mean contact pressure, p, could be obtained, as shown in the following equation:

$$p = \frac{F}{\pi RD/2}. \tag{9}$$

Note that the contact area used here is still the one predicted by Hertzian theory, which is underestimated since the strain has exceeded the elastic deformation regime.[41] Then, the Tresca criterion was used to correlate the mean contact pressure and the yield strength, Y. The Tresca criterion assumes that yielding occurs when the maximum shear stress (τ_{max}) has been reached.[45] According to the Tresca criterion, the relationship between the yield strength (Y), τ_{max}, and the principal stresses (σ_1, σ_2, and σ_3) is given by

$$Y = \max\{|\sigma_1 - \sigma_2|,\ |\sigma_2 - \sigma_3|, |\sigma_1 - \sigma_3|\} = 2\tau_{max}. \tag{10}$$

Then, the principal stresses and the maximum shear stress were calculated using Huber's method,[46] in terms of the mean contact pressure (p) (see Fig. S7 in the supplementary material for

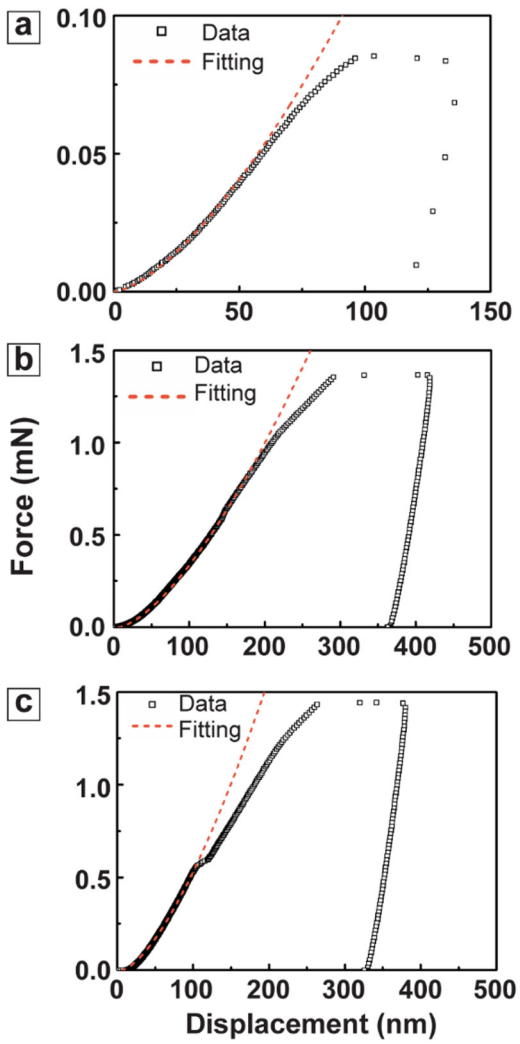

FIG. 5. Comparison of the experimentally measured force profiles (black hollow square) with those predicted by Hertzian theory in Eq. (7) (orange dashed line) for particles with different H content: (a) $Si_{0.5}H_{0.5}$, (b) $Si_{0.9}H_{0.1}$, and (c) $Si_{0.95}H_{0.05}$.

an example). The detailed calculation of the principal stresses and the maximum shear stress are also given in the supplementary material. The result is given in Eq. (11) where p and Y are related. The values of yield strength for three samples are listed in Table I,

$$Y = 0.66\,p. \tag{11}$$

E. Ultimate compressive strength

The values of the load and displacement corresponding to failure of the spheres are relatively easy to identify. However, obtaining the strength also requires the contact area at failure to be determined, which is not trivial given the preceding plastic deformation. Nonetheless, the Hertzian contact radius, Eq. (1), provides an upper bound for the compressive strength as it is an underestimate of the true contact area.[41] A different model—the cylinder model—was used to calculate the lower bound for the compressive strength.[41] In this model, the a-Si:H particle is considered to be a cylinder sitting on the substrate under compression with the upper surface fully contacting the flat tip surface, i.e., the contact area is the surface of the cylinder. During compression, in the cylinder model, the volume is assumed to be constant during the compression—the height of the cylinder decreases and the upper and lower surfaces expand. The contact radius in the cylinder model is

$$a_{\mathrm{cyl}} = \left(\frac{2R^3}{3(R-D)}\right)^{1/2}. \tag{12}$$

Among various models that can be used to calculate the contact area, the cylinder model predicts the largest contact area.[41] Therefore, the ultimate compressive strength from this model represents the lower bound. The range for ultimate compressive strength is shown in Table I.

Table I lists the diameter, maximum strain, Young's modulus, yield strength, and compressive strength measured for the three different a-Si:H samples, and the values reported for a-Si thin films and bulk c-Si. More than 10 particles from each sample were indented and fractured (see supplementary material for all of the force profiles). This decrease in Young's modulus is probably because H atoms disrupt Si–Si bonds and lead to more cavities inside the spheres, thereby reducing the density of the particles, which is also seen in a-Si:H thin films.[20,51,52] Note that the lower bound of the ultimate compressive strength is smaller than the yield strength for each a-Si:H particle. This can be attributed to two reasons. One is that the yield strength obtained from the deviation of linearity in the F vs $D^{3/2}$ curves is overestimated since the very initial plastic deformation may not be noticeable from the curve. The other reason is that the lower bound of the ultimate compressive strength predicted by the cylinder model is overestimated. To better understand the relationship between the H content of the spheres and their mechanical properties, molecular dynamics (MD) simulations were performed.

E. Molecular dynamics simulation

The details of the system preparation, force law, and simulation procedures are described in Experimental Details. Here, we focus on the results of the hydrogenation of Young's modulus of a-Si:H systems. Young's modulus of a-Si systems was determined from the stress-strain curve at small deformation ($\varepsilon_{\max} \sim 0.01$) under tensile deformation (see Fig. S8 in the supplementary material). Figure 6(a) shows the interphase formed by the clusters of H atoms in a-Si:H systems with different contents of H at $T = 300$ K. Simulation results show that above 30% H content, dispersed clusters of H atoms appear that can be considered as voids in the a-Si matrix. The volume fraction of these voids increases significantly only at a very high H content (50%) [see Fig. 6(a)]. The size of these voids is characterized by determining the size of each hydrogen cluster. Two hydrogen atoms belong to one cluster if

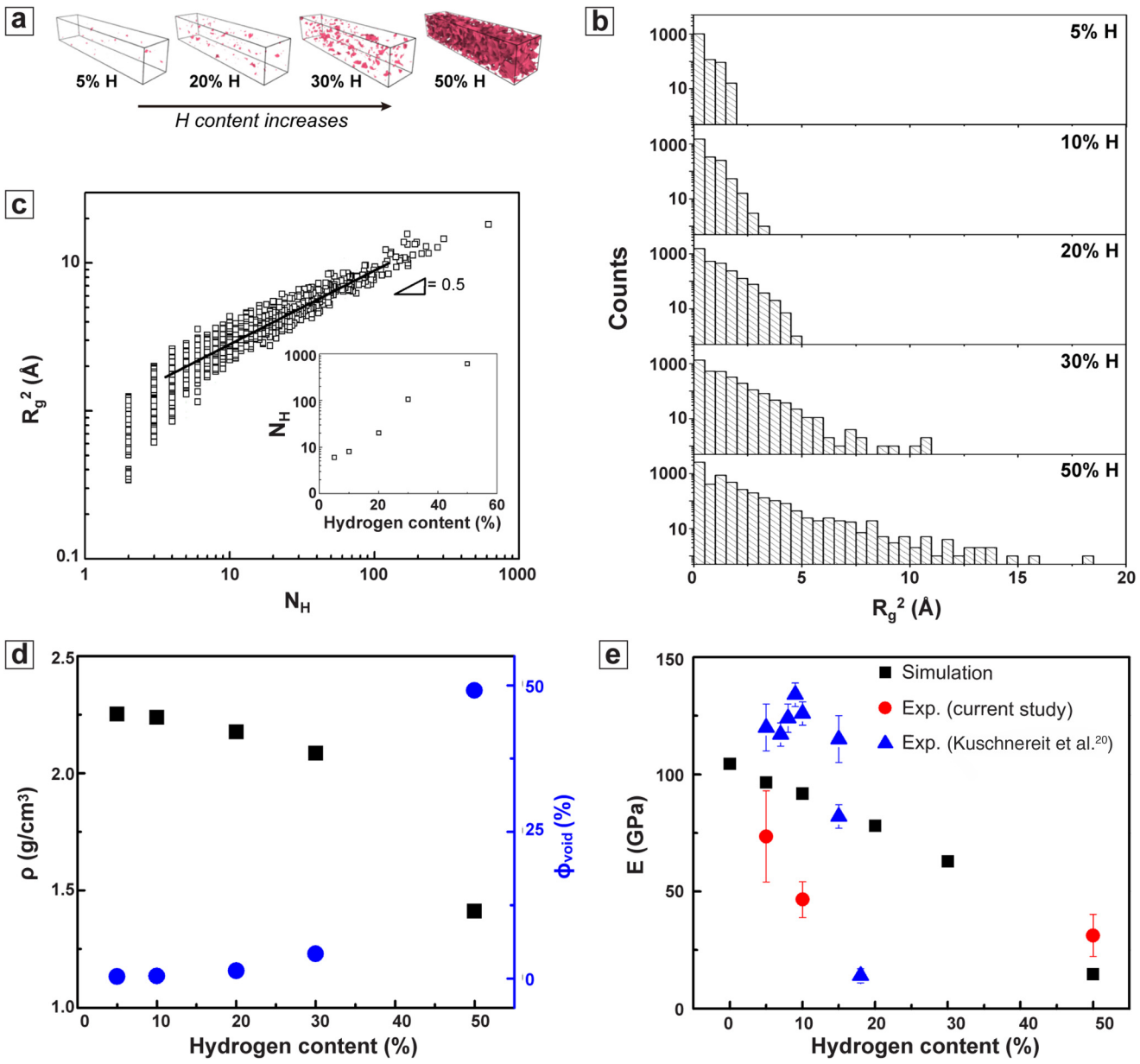

FIG. 6. (a) The interphase (red color) created by the clusters of H atoms in a-Si:H. (b) Distribution of the squared radius of gyration of the hydrogen clusters in a-Si:H with different H contents. (c) Square of radius of gyration as a function of the number of hydrogen atoms in each cluster. Inset: the number of hydrogen atoms in the largest cluster as a function of the hydrogen mole fraction. (d) Density (left axis) and volume fraction of H clusters or voids (right axis) as a function of the H mole fraction. (e) Comparison of Young's modulus of a-Si:H systems in the MD simulation (black squares), our experimental observation on a-Si:H particles (red circles), and surface acoustic wave spectroscopy characterization of a-Si:H thin films done by Kuschnereit *et al.*[20] (blue triangles).

their distance is less than 2.5 Å. The distribution of the squared radius of gyration of hydrogen atoms (R_g^2) is shown in Fig. 6(b) for different hydrogenation levels. The distribution of R_g^2 becomes wider as the hydrogen content increases. In Fig. 6(c) (we took a-Si:H with 50 at. % H content as an example), values of R_g^2 are plotted against the number of participating hydrogen atoms in each cluster, and a power-law behavior with an exponent of 0.75 is observed for R_g^2 as a function of the number of hydrogen atoms in each cluster N_H (i.e., $R_g^2 \sim N_H^{0.5}$). The inset of Fig. 6(c) shows the number of hydrogen atoms in the largest cluster ($N_{H,\,max}$) as a function of the

hydrogen content in a-Si:H MD samples, and as expected, the $N_{H,max}$ increases with the hydrogen content. The density (ρ) and volume fraction of these voids (ϕ) are shown as a function of the degree of hydrogenation in Fig. 6(d) at $T = 300$ K. Our simulation results for density of a-Si using the Tersoff potential[30,31] show a value of 2.27 g/cm^3, which is in good agreement with the experimental value of 2.285 g/cm^3.[53] The values of ϕ_{void} (right axis) increase with hydrogenation and in consequence the density (left axis) of a-Si:H systems decreases with increasing the H content as expected. In Fig. 6(e), the values of Young's modulus of the a-Si:H systems decrease with an increase in the hydrogenation in MD simulation, this experiment, and a-Si:H thin film experiment reported by Kuschnereit *et al.*[20] This decrease can be attributed to the emergence of several voids in the structure of a-Si that are created by the H atoms [see Figs. 6(a) and 6(b)] and the resulting lower densities as seen in Fig. 6(d). The difference in the MD results, our experimental observation on a-Si:H particles, and surface acoustic wave spectroscopy characterization of a-Si:H thin films[20] can stem from difficulties in determination of the exact H content, the presence of impurities, different characterizations, and geometry of a-Si:H systems. Lastly, although the force law[30,31] used in this study produces an excellent result for the density of the amorphous systems [see Fig. 6(b)], there still may be some inaccuracies associated with the force law in Young's modulus calculations in MD simulations. Nevertheless, the MD results clearly show that H atoms are capable of creating clusters in the a-Si phase, and the existence of these clusters can reduce Young's modulus of the system.

IV. CONCLUSIONS

The mechanical properties of a-Si:H particles have been characterized using a nanoindenter in conjunction with Hertz contact theory and MD simulations. The correlation between the mechanical properties and the H content has been found. With 5 at. % H content, Young's modulus is 73.5(±19.5) GPa, the yield strength is 5.8 GPa, and the compressive strength is 3.2(±0.1)–9.3(±0.6) GPa. However, when the H content increases to 50 at. %, Young's modulus, yield strength, and compressive strength decrease to 31.2 (±9.0) GPa, 2.5 GPa, and 1.8(±0.3)–5.3(±0.8) GPa, respectively. Furthermore, the MD simulations were utilized to understand the underlying mechanism of the decrease in Young's modulus of the a-Si:H systems. The simulation results showed that this decrease is associated with the clustering of the H atoms in a-Si. As the H content increases, the clusters become larger, and as a consequence, the density and Young's modulus of the network decrease. This work proves that compressing single particles with a nanoindenter with a flat probe tip is a promising method for the mechanical characterization of submicrometer-sized particles. Additionally, the H-dependent mechanical properties of a-Si:H particles can be important for their future applications.

SUPPLEMENTARY MATERIAL

See the supplementary material for XRD pattern, all nanoindentation curves, calculation of principal stresses, and maximum shear stress inside the a-Si:H particles; and simulation results.

ACKNOWLEDGMENTS

We acknowledge funding of this work by the Robert A. Welch Foundation (Grant No. F-1464) and the Center for Dynamics and Control of Materials (CDCM) supported by the National Science Foundation (NSF) under NSF Award No. DMR-1720595.

REFERENCES

[1]L. E. Pell, A. D. Schricker, F. V. Mikulec, and B. A. Korgel, Langmuir **20**, 6546 (2004).
[2]J. T. Harris, J. L. Hueso, and B. A. Korgel, Chem. Mater. **22**, 6378 (2010).
[3]L. Shi, J. T. Harris, R. Fenollosa, I. Rodriguez, X. Lu, B. A. Korgel, and F. Meseguer, Nat. Commun. **4**, 1904 (2013).
[4]L. Lin, S. Lepeshov, A. Krasnok, T. Jiang, X. Peng, B. A. Korgel, A. Alù, and Y. Zheng, Materials Today **25**, 10–20 (2019).
[5]S. Lepeshov, M. Wang, A. Krasnok, O. Kotov, T. Zhang, H. Liu, T. Jiang, B. Korgel, M. Terrones, Y. Zheng, and A. Alú, ACS Appl. Mater. Interfaces **10**, 16690 (2018).
[6]M. L. De Marco, S. Semlali, B. A. Korgel, P. Barois, G. L. Drisko, and C. Aymonier, Angew. Chem. Int. Ed. **57**, 4478 (2018).
[7]S. Murugesan, J. T. Harris, B. A. Korgel, and K. J. Stevenson, Chem. Mater. **24**, 1306 (2012).
[8]M. T. McDowell, S. W. Lee, J. T. Harris, B. A. Korgel, C. Wang, W. D. Nix, and Y. Cui, Nano Lett. **13**, 758 (2013).
[9]B. R. Neugirg, S. R. Koebley, H. C. Schniepp, and A. Fery, Nanoscale **8**, 8414 (2016).
[10]E. P. S. Tan and C. T. Lim, Appl. Phys. Lett. **87**, 123106 (2005).
[11]A. Heidelberg, L. T. Ngo, B. Wu, M. A. Phillips, S. Sharma, T. I. Kamins, J. E. Sader, and J. J. Boland, Nano Lett. **6**, 1101 (2006).
[12]S. M. Kim, A. Hsu, M. H. Park, S. H. Chae, S. J. Yun, J. S. Lee, D.-H. Cho, W. Fang, C. Lee, T. Palacios, M. Dresselhaus, K. K. Kim, Y. H. Lee, and J. Kong, Nat. Commun. **6**, 8662 (2015).
[13]J. Tao, W. Shen, S. Wu, L. Liu, Z. Feng, C. Wang, C. Hu, P. Yao, H. Zhang, W. Pang, X. Duan, J. Liu, C. Zhou, and D. Zhang, ACS Nano **9**, 11362 (2015).
[14]J. W. Suk, R. D. Piner, J. An, and R. S. Ruoff, ACS Nano **4**, 6557 (2010).
[15]C. Lee, X. Wei, J. W. Kysar, and J. Hone, Science **321**, 385 (2008).
[16]A. L. Weisenhorn, M. Khorsandi, S. Kasas, V. Gotzos, and H.-J. Butt, Nanotechnology **4**, 106 (1993).
[17]S. Zou, H. Schönherr, and G. J. Vancso, Angew. Chem. **117**, 978 (2005).
[18]F. M. Hecht, J. Rheinlaender, N. Schierbaum, W. H. Goldmann, B. Fabry, and T. E. Schäffer, Soft Matter **11**, 4584 (2015).
[19]Q. S. Li, G. Y. H. Lee, C. N. Ong, and C. T. Lim, Biochem. Biophys. Res. Commun. **374**, 609 (2008).
[20]R. Kuschnereit, H. Fath, A. A. Kolomenskii, M. Szabadi, and P. Hess, Appl. Phys. A **61**, 269 (1995).
[21]D. M. Follstaedt, J. A. Knapp, and S. M. Myers, J. Mater. Res. **19**, 338 (2004).
[22]J. Gaspar, O. Paul, V. Chu, and J. P. Conde, MRS Proc. **1066**, 1066 (2008).
[23]L. B. Freund and S. Suresh, *Thin Film Materials Stress, Defect Formation and Surface Evolution* (Cambridge University Press, Cambridge, 2004).
[24]S. M.-M. Dubois, G.-M. Rignanese, T. Pardoen, and J.-C. Charlier, Phys. Rev. B **74**, 235203 (2006).
[25]G. Stan, S. Krylyuk, A. V. Davydov, I. Levin, and R. F. Cook, Nano Lett. **12**, 2599 (2012).
[26]J. Gaspar, O. Paul, V. Chu, and J. P. Conde, J. Micromech. Microeng. **20**, 035022 (2010).
[27]E. Johlin, N. Tabet, S. Castro-Galnares, A. Abdallah, M. I. Bertoni, T. Asafa, J. C. Grossman, S. Said, and T. Buonassisi, Phys. Rev. B **85**, 075202 (2012).
[28]C. L. Yaws, *The Yaws Handbook of Thermodynamic Properties for Hydrocarbons and Chemicals* (Gulf Publishing, 2006).
[29]O. L. Guise, J. W. Ahner, M.-C. Jung, P. C. Goughnour, and J. T. Yates, Nano Lett. **2**, 191 (2002).

[30]J. Tersoff, Phys. Rev. B **39**, 5566 (1989).
[31]J. Tersoff, Phys. Rev. B **37**, 6991 (1988).
[32]F. Khabaz and R. Khare, J. Phys. Chem. B **119**, 14261 (2015).
[33]F. Khabaz, Y. Zhang, L. Xue, E. L. Quitevis, E. J. Maginn, and R. Khare, J. Phys. Chem. B **122**, 2414 (2018).
[34]P. Biswas, R. Atta-Fynn, and S. R. Elliott, Phys. Rev. B **93**, 184202 (2016).
[35]S. Plimpton, J. Comput. Phys. **117**, 1 (1995).
[36]G. D. Cody, T. Tiedje, B. Abeles, B. Brooks, and Y. Goldstein, Phys. Rev. Lett. **47**, 1480 (1981).
[37]A. P. Sokolov, A. P. Shebanin, O. A. Golikova, and M. M. Mezdrogina, J. Phys. Condens. Matter **3**, 9887 (1991).
[38]C. Grein, P. Béguelin, and H-H Kausch, in *European Structural Integrity Society*, edited by B. R. K. Blackman, A. Pavan, and J. G. Williams (Elsevier, 2003), pp. 129–141.
[39]T. Ando, K. Sato, M. Shikida, T. Yoshioka, Y. Yoshikawa, and T. Kawabata, in *1997 International Symposium on Micromechanics and Human Science (Cat. No.97TH8311)* (IEEE, 1997), pp. 55–60.
[40]S. Johansson, J. Schweitz, L. Tenerz, and J. Tirén, J. Appl. Phys. **63**, 4799 (1988).
[41]J. Paul, S. Romeis, J. Tomas, and W. Peukert, Adv. Powder Technol. **25**, 136 (2014).
[42]H. Hertz, J. Reine Angew. Math. **9**, 156 (1882).
[43]C.-H. Hsueh and P. Miranda, J. Mater. Res. **19**, 2774 (2004).
[44]R. L. C. Vink, G. T. Barkema, W. F. van der Weg, and N. Mousseau, J. Non Cryst. Solids **282**, 248 (2001).
[45]H. Tresca, C. R. Acad. Sci. IIA **59**, 754 (1864).
[46]M. T. Huber, Ann. Phys. **319**, 153 (1904).
[47]L. A. Berla, S. W. Lee, I. Ryu, Y. Cui, and W. D. Nix, J. Power Sources **258**, 253 (2014).
[48]W. N. Sharpe, B. Yuan, R. Vaidyanathan, and R. L. Edwards, in *Proceedings IEEE The Tenth Annual International Workshop on Micro Electro Mechanical Systems. An Investigation of Micro Structures, Sensors, Actuators, Machines and Robots* (IEEE, 1997), pp. 424–429.
[49]T. Yi, L. Li, and C.-J. Kim, Sens. Actuators A **83**, 172 (2000).
[50]*Engineering Properties of Selected Ceramic Materials*, edited by J. F. Lynch, C. G. Ruderer, W. H. Duckworth, Battelle Memorial Institute, and American Ceramic Society (American Ceramic Society, Columbus, OH, 1966).
[51]P. Biswas and D. A. Drabold, "Correlations between higher-order rings and microvoids in hydrogenated amorphous silicon," MRS Online Proc. Libr. Archive 1757 (published online).
[52]P. Biswas, D. Paudel, R. Atta-Fynn, D. A. Drabold, and S. R. Elliott, Phys. Rev. Appl. **7**, 024013 (2017).
[53]J. S. Custer, M. O. Thompson, D. C. Jacobson, J. M. Poate, S. Roorda, W. C. Sinke, and F. Spaepen, Appl. Phys. Lett. **64**, 437 (1994).